Development of Interactive Systems for Digital Art Exhibitions Integrating Neural Radiance Fields

Lu Yang
Department of Digital Media Art, Academy of Fine Arts, Changchun normal University, Changchun 130032, Jilin, China
Corresponding author: Lu Yang (e-mail: stranger_0710@163.com)

ABSTRACT To foster a new paradigm for immersive digital art exhibitions that integrate virtual and real interactions, this paper designs and develops an interactive system integrating Neural Radiance Fields (NeRF), enabling realistic 3D visualization of textile designs and historical garments. As high-fidelity scene reconstruction and interactive rendering are increasingly important for electromagnetic information visualization, digital twins, and intelligent sensing applications, the proposed framework provides a practical reference for multimodal spatial representation and high-dimensional field reconstruction. The system effectively addresses the core challenges of dynamic representation of textile artworks and insufficient real-time interactivity through an interactive perception layer, a core processing layer, and a rendering and display layer. Users provide gesture, touch position, and pressure signals via a high-precision capacitive touchscreen to drive physically consistent interactions. The core innovation combines hash-encoded NeRF with a physically aware deformation network through an end-to-end differentiable joint optimization architecture, tightly coupling textile mechanical properties with high-dimensional visual representations to achieve consistency between geometric deformation and optical rendering. A hierarchical query mechanism and adaptive update strategy further enable real-time closed-loop interaction from user input to high-fidelity image generation. Experimental results demonstrate a rendering latency of 41.9 ms $\pm$ 9.8 ms with 23.9 $\pm$ 2.1 FPS under dynamic scaling, while achieving LPIPS of 0.31 $\pm$ 0.06 and SSIM of 0.75 $\pm$ 0.04 under high wind loads, providing both visual realism and interactive smoothness for immersive digital exhibition systems.

INDEX TERMS neural radiance fields, interactive system, hash encoding, electromagnetic information visualization, intelligent sensing

I. INTRODUCTION

TO achieve highly realistic, real-time interactive displays of textile artworks, it is urgent to build an integrated system that can dynamically respond to user input and form a closed-loop feedback loop [1-2]. As an artistic medium with rich topological structures and tactile semantics, textiles carry dual information flows of mechanics and aesthetics during their deformation process [3]. Neural radiance fields reconstruct spatial radiation characteristics through implicit functions, providing a continuous expression basis for high-dimensional visual data [4-6]. Embedding physical laws into this framework can not only enhance the visual realism of virtual materials under interactive perturbations, but also achieve computational modeling of the evolution of artistic forms, expand the technical boundaries of virtual-reality interaction in immersive exhibitions, and promote the development of digital art towards the integration of embodied cognition and multimodal perception.

Current reconstruction methods based on implicit neural representations face the problem of decoupling geometric evolution from appearance rendering when dealing with flexible materials such as textiles [7-8]. Most models treat deformation as a learning task independent of the radiation field and lack explicit modeling of internal stress transfer mechanisms, making displacement predictions solely data-driven and difficult to generalize to unseen perturbation patterns [9-10]. When local stretching and wrinkling occur, the difference between surface normals and texture stretching can produce visual artifacts [11-12]. Furthermore, the efficiency of prior encoding methods for high-dimensional spatial coordinates is a bottleneck for existing methods. Dynamic scenes cause frequent updates of volume density, resulting in intensive computation and high inference latency, hindering real-time and interactive experiences [13-14]. As a side effect, another debate in deformation processes is the diminishing influence of innate material properties. Properties such as Density, Young's Modulus, and Poisson's ratio are often ignored when optimizing networks, introducing unrealistic simulation behavior to the optimizer [15-16]. Many methods also introduce spring-mass systems with constraints, but their discontinuities are often inconsistent with the gradient returns in the implicit field or with the rendering techniques [17-18]. As a result, visual realism and structural complexity are lost, leading to unnatural “floating” and “jittering” of dynamic details [19-20], ultimately compromising the precise emotional expression of the artwork.

This paper proposes an interactive system combining hash-coded NeRF and a physically aware deformation network for ultra-realistic visualization of textile materials under dynamic perturbations. An end-to-end differentiable joint optimization scheme is also introduced. Based on linear elasticity, the deformation displacement field is solved via differential equations and injected as a conditional signal into the hash-coded spatial coordinate embedding, enabling the radiation field to detect changes in the local mechanical state. The physical properties of fabrics are incorporated into the deformation network architecture, enabling the model to learn how to differentiate the responses of different fabrics. In the MLP (Multi-Layer Perceptron) decoding stage, a normal continuity loss is applied to maintain surface smoothness. In this case, a stress-strain consistency regularization term is constructed to force the network output to conform to the basic laws of Hooke’s law, which can, to a certain extent, ensure the consistency of geometric deformation and optical rendering. The entire system supports the recovery of high-resolution dynamic details from sparse observations and implements backpropagation optimization through differentiable rendering, improving reconstruction speed and stability. This method not only enhances the visual credibility of digital art exhibits during the interactive process, but also provides a complete set of technical solutions and system implementations for the physical compliance animation of flexible objects, promoting the evolution of virtual-reality fusion exhibition technology to a higher level of realism, intelligence, and deployability.

II. DESIGN AND IMPLEMENTATION OF INTERACTIVE EXHIBITION SYSTEMS INTEGRATING NEURAL RADIANCE FIELDS

Figure 1 illustrates a neural radiation field-based mass interaction system for digital art exhibitions. User input drives the physical deformation network, which, combined with material parameters, generates a displacement field through an elastic mechanics model [21-22]. Multi-scale hash coding efficiently extracts features from spatial coordinates, capturing both the global topology and local details of the fabric. The deformed features are fed into a neural network to predict density and color, respectively, and volume rendering produces a high-fidelity image [23-24]. This system forms a closed-loop from interaction to rendering, ensuring deformation authenticity and visual consistency through physical constraints, enabling immersive displays of digital textile artworks under dynamic perturbations.

A. SYSTEM DESIGN GOALS AND OVERALL ARCHITECTURE

To construct an efficient implicit representation for high-dimensional visual data in digital art exhibitions, this study designs a multi-scale neural radiance field modeling mechanism based on hash coding [25-26]. This structure takes spatial coordinates as input and embeds them into L learnable hash tables with different resolutions through a hierarchical hash mapping strategy. Each hash table is divided into a fixed number of buckets, whose index is generated by a parameterized hash function of the form:

$$h_l(x) = \mathrm{Hash}_l\left(\left\lfloor x \cdot 2^{b_l} \right\rfloor\right) \bmod T_l \tag{1}$$

x represents the coordinates of the sampling points in three-dimensional space; 2^{b_l} controls the spatial partitioning granularity of layer l and determines the scaling factor of the coordinates; T_l is the total number of slots in the hash table of layer l. This hash function is differentiable, allowing gradients to be backpropagated to the coordinate input during training, thus supporting end-to-end optimization. Each hash table layer stores a set of low-dimensional feature vectors. After the input position is located by the hash function, features are queried from the respective slots, and bilinear interpolation is applied to combine the contributions of neighboring grid cells, enhancing the smoothness of the spatial representation.

The extracted features at each level are normalized and concatenated to form a high-dimensional joint embedding $e(x) = [f_1; f_2; \ldots; f_l]$, where f_l represents the feature vector output by the hash table at level l. This joint embedding serves as the initial input to a multi-layer perceptron (MLP), driving the subsequent nonlinear transformation process. The MLP first decodes the density signal $\sigma(x)$ through several fully connected layers, reflecting the local spatial opacity distribution. Subsequently, under the condition of viewing direction, RGB (Red, Green, Blue) color values are further predicted by combining viewpoint related feature branches. The entire forward inference process fully utilizes the sparse activation characteristics of the hash structure, significantly reducing memory access redundancy while preserving subvoxel-level geometric details. To address the high-frequency information modeling challenges presented by the complex surface textures of textile exhibits, the resolution of each hash table increases exponentially. The bottom layer focuses on capturing global topology, while the higher layers focus on reconstructing local wrinkles and texture details. Furthermore, a gradient masking mechanism is applied to limit parameter updates in invalid regions [27-28]. Only key sampling points along the ray path are returned for feature extraction, effectively reducing the computational load.

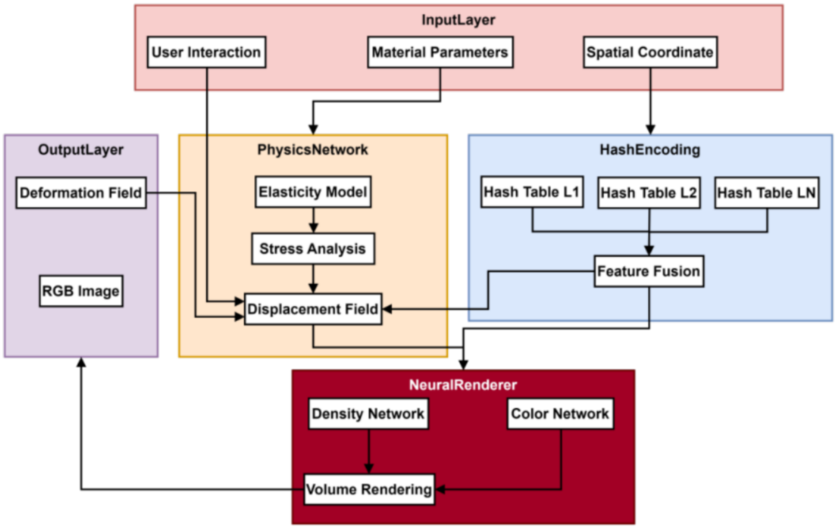

FIGURE 1. Interactive system based on neural radiation field

B. MULTIMODAL INTERACTIVE PERCEPTION HARDWARE DESIGN AND INTERACTIVE PERCEPTION LAYER

To achieve physical compliance deformation modeling of textile materials during dynamic interactions, this study constructs a deformation network structure based on the continuum mechanics framework. Its core mechanism relies on the linear elastic theory to impose differential constraints on local geometric evolution [29-30]. The network takes the initial spatial position as input and outputs the displacement vector field of the corresponding point under external perturbations. The parameters are jointly optimized through a differentiable architecture and a radiation field model. The deformation behavior is dominated by the stress-strain relationship, where the Cauchy stress tensor is related to the strain field through the generalized Hooke's law:

$$\sigma = \lambda(\nabla \cdot u)I + \mu\left(\nabla u + (\nabla u)^T\right) \tag{2}$$

In the formula, λ and μ are the Lame constants, derived from the inherent material properties of mass per unit area, Young's modulus, and Poisson's ratio. These parameters are incorporated as prior information in the network weight initialization and loss formation, allowing the model to distinguish between the mechanical behavior of different fabric materials (e.g., silk, cotton, and linen). Although the Lamé constant is derived from linear elasticity theory, the deformation network learns residual deformation from real fabric motion data through differentiable training, thereby effectively compensating for material anisotropy and nonlinear behavior under large deformation. The strain tensor is derived from the gradient of the displacement field, ensuring that the local deformation satisfies symmetry and continuity conditions under the assumption of small strains. Although the fundamental physical model is based on small-strain linear elasticity theory, through end-to-end differentiable training, the deformation network can learn nonlinear response characteristics from the data, thereby achieving an effective approximation of the behavior of real fabrics in large deformation regions.

At the network implementation level, the displacement field prediction adopts a lightweight fully connected network structure. The input is a high-dimensional embedding representation of the spatial coordinates after hash coding, and the output is a three-dimensional displacement component [31-32]. To ensure the energy rationality of the deformation process, an internal force balance regularization term based on the principle of virtual work is applied, and a static residual constraint is imposed on each point during the training process:

$$\mathcal{L}_{mech} = \int_{\Omega} \left\|\nabla \cdot \sigma + f_{ext}\right\|^2 dx \tag{3}$$

Ω represents the spatial domain occupied by the object, and f_{ext} is the density of external forces (such as the local pressure caused by a user touch). It uses automatic differentiation to calculate the second-order derivatives of the displacement field, thereby calculating the stress divergence, and discretizes the solution to a set of spatial points using Monte Carlo sampling. This physical loss term effectively participates in the backpropagation flow, forcing the network to output a displacement solution that satisfies mechanical equilibrium, thus preventing unphysical vibrations or energy accumulation.

Furthermore, the deformed world position is mapped back to the radiation field query path as a reference coordinate to predict color and density. In this process, the surface normal can also be explicitly calculated from the gradient of the deformation implicit field [33-34]. Since the displacement field and the radiation field are optimized for the same goal, the normal evolution is naturally coupled with the strain state, so that the visual effects caused by texture stretching, wrinkle formation, etc., are faithful to the inherent stress distribution [35-36].

C. CORE PROCESSING ALGORITHM BASED ON PHYSICAL DEFORMATION - NERF

To balance the real-time rendering requirements of highly dynamic textile materials in interactive scenes such as digital art exhibitions, a hierarchical hashing multi-granularity volume query pipeline is proposed. This pipeline leverages computational optimizations in both space and time to achieve efficient and differentiable rendering. The scheme comprises a two-stage sampling approach that operates on a set of points unevenly distributed along a ray path. In a first pass, a coarse-grained scan of the scene is performed from a low-resolution hash hierarchy. Each hash bucket corresponds to a fairly big spatial voxel cell so that the strength of the local density response can be rapidly evaluated. The system, along the parameterized ray trajectory, performs discrete sampling with adaptive step size and calls a lightweight decoding network to produce coarse density estimates. When the density of a number of consecutive sample points is below a certain threshold, the fragment is considered to be empty, and skip integration is applied to bypass subsequent high-cost queries. Once a potential surface is found, the system automatically switches to fine-scale query mode by turning on a high-resolution hash table, which resamples densely at the subdomain inside the critical interval. A reduced step size is then used along with an importance sampling scheme to concentrate more points near regions of high gradient variation to capture small geometrical details like fabric wrinkles and curvature of the edge. The sampling points in the fine-scale stage are embedded via multi-level hashing and passed to the full MLP branch, which returns high-fidelity color and density. Pixel synthesis can be completed through the cumulative integral formulas:

$$C(r) = \sum_{i=1}^{N} T_i \left(1 - \exp(-\sigma_i \delta_i)\right) c_i \tag{4}$$

$$T_i = \exp\left(-\sum_{j=1}^{i-1} \sigma_j \delta_j\right) \tag{5}$$

$C(r)$ is the color value rendered along the ray r; N is the total number of samples; σ_i and c_i are the density and color of the i-th point, respectively; δ_i is the spacing between adjacent samples; T_i is the transmittance, reflecting the attenuation of the visibility of the current point by the preceding medium.

Temporal stability and between-frame performance are further improved by a integrated ray cache module. This entails storing the key sample positions plus related hash address indices for each primary ray from the last frame. Rendering further frames is initiated by predicting the geometric layout of the current view from the camera motion vector and the user's perturbation signal. This initial guess is roughly based on the sampling distribution of similar rays stored in the cache. The spatiotemporal coherence compensation component adjusts the resampling range by comparing the hash signature cosine between two consecutive frames. When similarity is high, path reconstruction is simplified to local path reconstruction at significant displacements, patching similar patches at the same locations on the old path; otherwise, global path reconstruction is performed. This is achieved by using a cache queue in the GPU (graphics processing unit) shared memory, ensuring sub-millisecond data reuse latency. In fact, the CUDA architecture designs the entire rendering process for asynchronous scheduling, performing coarse screening, fine checking, and cache retrieval as three independent computational processes to fully utilize the computing power of modern graphics cards.

D. RENDERING AND DISPLAY OUTPUT LAYER

To achieve a dynamic balance between responsiveness and visual fluency during human-computer interaction in digital art exhibitions, an update strategy based on multimodal input analysis and adaptive computational load scheduling is employed. The system's front-end combines a high-precision capacitive touchscreen with a small inertial measurement unit (IMU) to acquire real-time user contact position, pressure gradient, and gesture trajectory on the virtual exhibit surface. The touchscreen and IMU are aligned via hardware-level timestamps (accuracy ± 0.1 ms) and interpolated at a uniform sampling rate of 1 kHz at the driver layer to ensure the spatiotemporal consistency of the spatial perturbation field. The raw signals are then denoised and registered with a low-latency filter. The acquired operation data is converted into a continuous spatial disturbance field p(x,t) through a nonlinear mapping function. Its amplitude is determined by the ratio of local pressure to the area of action, and its direction is determined by the finger slip vector or the rate of change of the device's attitude angle, forming a physically meaningful external force density input.

The disturbance field is passed to the decision module to determine the impact of the current interaction behavior on the geometry. The system calculates a differentiable response strength indicator defined as:

$$I_{int} = \alpha \int_{\Omega_p} \|\nabla \cdot p(x,t)\| \, dx + \beta \max_{x \in \Omega_p} \|p(x,t)\| \tag{6}$$

Ω_p represents the spatial support domain of the warped region, and α and β are normalized weighting factors that modify the ratio of the appearance term to the peak force term, respectively. This metric accounts for both the spatial concentration and mechanical strength of the perturbation, and is therefore a potential criterion for determining global model reoptimization. When I_{int} exceeds the preset threshold, the system detects a large deformation event, triggering backpropagation of gradients for the affected hash table entries and their adjacent entries, and incrementally updates the relevant local MLP weights instead of performing global retraining. Otherwise, it enters a local fine-tuning mode, locking only the affected hash bucket and its neighboring nodes. An incremental gradient descent algorithm is applied to update the local MLP weights to avoid the cost of global backpropagation.

In the temporal domain, the system dynamically adjusts the inference frequency of the deformation network based on the difference in the perturbation fields between previous and subsequent frames. When the rate of change falls below a certain steady-state threshold, the execution cycle is doubled to once every three frames, and the smooth evolution of the displacement field is compensated for through interpolation. They then check for bursty conditions, and if a bursty operation is detected, they immediately resume frame-by-frame inference and increase the bandwidth of hash feature updates. Simultaneously, the rendering pipeline synchronously adjusts its sampling strategy: to reduce redundant queries, ray cache reuse is activated under weak perturbations; under strong perturbations, full-path resampling is enabled to ensure geometric fidelity.

III. SYSTEM PERFORMANCE EXPERIMENT

A. RENDERING EFFICIENCY AND REAL-TIME

In the case of a 512×512 resolution display, the proposed NeRF is compared with NeRF, Instant-NGP (Instant Neural Graphics Primitives), and Plenoxels in terms of single-frame rendering time (ms) and frames per second (FPS). Experiments are conducted in both static view browsing and dynamic gesture scaling to measure rendering efficiency.

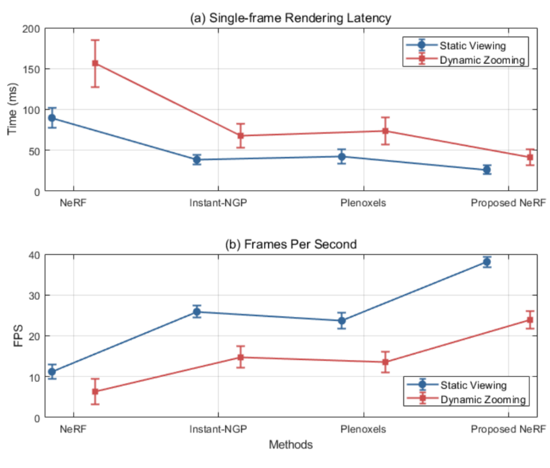

FIGURE 2. Rendering efficiency: (a) is single-frame rendering time; (b) is corresponding FPS. Error bars reflect the variance in performance

In static view, all approaches are highly stable. The proposed method enables substantial computation reduction, attaining the minimum latency and maximum frame rate, by the virtue of the hierarchical hash query with lightweight deformation coupling scheme. With dynamic gesture interaction, the geometry of the scene is in a state of continuous change. Traditional approaches need to regenerate the implicit field or modify the voxel structure on a regular basis, which leads to a drastic increase in rendering time and a significant reduction in the frame rate. NeRF specifically is bottlenecked by repeated inferences in the global MLP, limiting its responsiveness. In contrast, the proposed system adopts a adaptive local update scheme and carries out incremental optimization only in the disturbed area. It also re-utilizes the previous sampling information combined with predictions of spatiotemporal coherence efficiently to mitigate the exponential increment of computation costs. Under dynamic scaling, the average time for single-frame rendering is 41.9 ms ± 9.8 ms with an FPS of 23.9 ± 2.1. Moreover, the parametric representation of the physically aware deformation network that underlies the performance analysis reduces dependence on retraining and enables smoother performance degradation in dynamic modes. The performance deviation of the two modes demonstrates how different architectures adapt differently to dynamic input. While preserving visual quality, this approach facilitates the joint optimization of interactive real-time performance and computational efficiency, demonstrating its strengths in applications with high-dynamic digital art exhibition.

It should be noted that this system is designed for digital art exhibition scenarios that prioritize aesthetic experience and consistency in physical response, rather than applications such as high-speed action games or virtual reality headsets that are extremely sensitive to frame rates. In exhibition environments dominated by static or slowly changing interactions, 20–25 FPS can provide acceptable smoothness, especially when the content has high-fidelity detail and smooth motion. Furthermore, the system effectively suppresses inter-frame jitter through spatiotemporal consistency compensation and interpolation mechanisms, further enhancing the subjective sense of smoothness.

B. DYNAMIC DEFORMATION VISUAL REALITY ASSESSMENT

Using LPIPS (Learned Perceptual Image Patch Similarity) and SSIM (Structural Similarity Index) as visual fidelity metrics, the accuracy of dynamic deformation detail restoration is quantified. It should be noted that LPIPS and SSIM are used here to measure the perceptual and structural similarity between the rendered result and the reference video sequence, reflecting the system's ability to maintain visual realism under dynamic perturbations, rather than directly quantifying mechanical accuracy; physical plausibility is guaranteed by the differential constraints and regularization terms in the deformation network during the training phase. The proposed NeRF system is compared with NeRF, Instant-NGP, and Plenoxels in simulated sequences of typical textile motions, such as the fluttering of silk and the unfolding of woolen folds. The experiments are conducted under three wind disturbance levels (low, medium, and high).

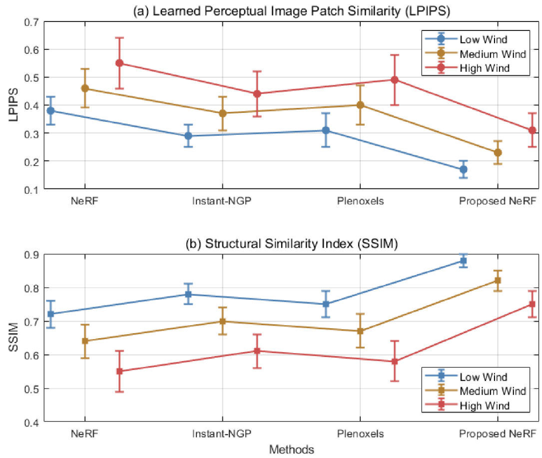

FIGURE 3. Accuracy evaluation of dynamic deformation detail restoration: (a) shows the trend of the LPIPS index as a function of airflow intensity; (b) shows the distribution of SSIM scores

Figure 3 demonstrates the ability of different neural rendering methods to reproduce the dynamic deformation details of textile materials under multiple levels of wind disturbance. Figure 3 (a) shows the trend of the LPIPS index as a function of airflow intensity. The proposed system maintains the lowest perception distance under low to high wind load conditions, reaching 0.31 ± 0.06 under high wind load conditions. This indicates that its generated images are more semantically accurate to the texture evolution of real fabric motion, attributed to the physical perception deformation network's modeling of the mechanical constraints of fiber stretching and wrinkle propagation. In contrast, other methods exhibit significant deviations under high disturbances, reflecting visual distortion caused by the geometry-appearance decoupling. Figure 3 (b) shows the distribution of SSIM scores. The proposed NeRF maintains the highest structural fidelity across various wind conditions, reaching 0.75 ± 0.04 under high wind load conditions. This demonstrates that the hash coding and hierarchical query mechanism effectively preserve local contrast and edge continuity. The changing gradients of the three lines reveal that when external excitation increases, methods lacking physical priors find it difficult to coordinate surface normals and illumination consistency, resulting in a rapid decay of structural similarity. However, this method, through the stress-strain regularization term and the joint optimization strategy, can maintain a stable spatially coherent expression even when deformation intensifies, thereby achieving high-fidelity reproduction of the dynamic evolution of the texture of artistic fabrics.

C. COMPARISON OF SYSTEM COMPUTING RESOURCE CONSUMPTION

To fully investigate the resource consumption of different implicit neural representation techniques in the context of digital art exhibitions, a multi-dimensional storage and computational overhead comparison test is developed. A training set is formed using high-resolution scan sequences of representative textile samples as input to provide uniform conditions. To prevent additional bias due to differences in sparsification strategies, all methods adopt feature encoding optimization with the same compression rate. The total number of parameters of the model is counted in millions, and the peak GPU memory usage during training is reported in gigabytes as a proxy for hardware resource consumption. The number of iterations to reach a given loss threshold is also recorded to quantify the optimization efficiency. The average memory bandwidth (GB/s) is sampled via performance counters on the GPU to assess the pressure of data transfer.

TABLE 1. Comparison of computing resource consumption

Method	Total Parameters (M)	Peak GPU Memory Usage (GB)	Convergence Iterations	Average Memory Bandwidth (GB/s)
NeRF	128.5	14.6	300	385
Instant-NGP	42.7	7.3	40	520
Plenoxels	68.9	8.1	50	410
Proposed NeRF	39.2	6.8	45	490

Table 1 systematically compares the computational resource consumption characteristics of different neural implicit representation methods in digital art exhibition scenarios. This system significantly outperforms traditional NeRF in terms of total parameters (39.2M) and peak GPU memory usage (6.8 GB). This is attributed to the hash-coded sparse activation mechanism, which effectively compresses spatial representation redundancy and avoids over-parameterization of high-dimensional coordinates in fully connected networks. Compared to Instant-NGP and Plenoxels, this method shares the underlying radiation field structure through a physically aware deformation network, applying mechanical constraints without significantly increasing model size, demonstrating the advantages of a compact architecture design. The convergence iteration count is close to that of Instant-NGP, indicating that the multi-scale hash index maintains fast optimization capabilities, while the application of the physical regularization term does not significantly reduce training efficiency.

D. INTERACTION LATENCY AND RESPONSE CONSISTENCY TEST

In this paper, end-to-end latency (ms) refers to the time from user input to screen update completion. Various network load scenarios (local offline, LAN transmission, and cloud inference) are evaluated; the latency standard deviation and jitter are quantified; the stability of the model in various terminal environments is verified.

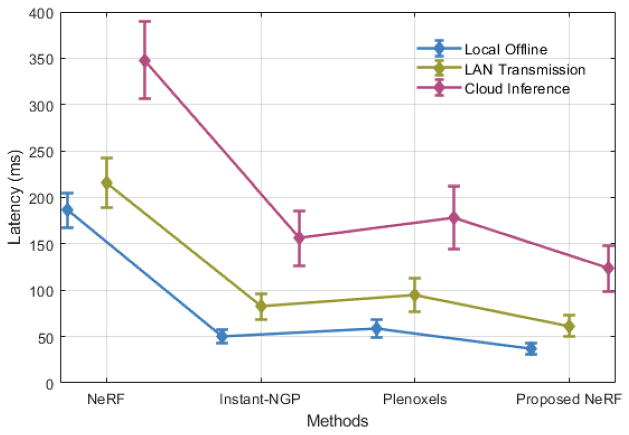

FIGURE 4. End-to-end interaction latency across deployment modes

Note: LAN stands for Local Area Network

The whole view of neural rendering methods' interactive response latency under various deployment scenarios is depicted in Figure 4. Through three load scenarios of network conditions, (the local offline, the LAN transmission, and the cloud-based), the proposed NeRF model shows the absolute lowest latency with the average 36.5ms-123.7ms, slight fluctuation, and excellent stability by the response. This value also comes from the proposed method's highly compacted hash-coded model structure that is combined with the optimization of a multi-layer rendering pipeline, which is not only scalable but also more efficient to do data processing and transmission. Classical NeRF models are equipped with a multitude of parameters and complex global query habit, meaning that substantial communication overhead and queuing delays are likely to occur for long distances. Although Instant-NGP and Plenopixels are able to enable instantaneous local inference, they fail to address the issues of buffering and state synchronization, which mitigate the effects of network instability and result in high latency. The travel times of these methods are affected by the changes in these environments from local to cloud environments. The design of the new NeRF model is also remarkable for its separation of the task of predicting physical deformation from the updates of the radiation fields; local incremental updates are possible and the influence of high-latency links on interactive fluidity becomes less problematic.

IV. CONCLUSION

This study creates a NeRF's and PPDN's hash-coded form neural radiance fields (learning from the requirement of extremely high-fidelity flexible textile simulation) that require physically perceptual deformations during dynamic perturbations. In its practical implementation, differential constraints obtained from linear elasticity are exploited to apply innate parameters of the fabric during training, which in turn help to study both the geometric changes and the stress distribution. The end-to-end, mathematically valid, coupling between the radiance field and the deformation network scientifically enables surface normal and texture elongation in the dynamic world. The merging of the hierarchical query strategy, which works in concert with adaptive update scheduling, creates the system that can effectively retain the desired rendering quality. The idea behind the proposed framework is to turn digital art exhibitions from mere static views into concrete representations of numbers and formulas. It is a concept that can not only help visualize the physically impossible flexible structures but also can enable to run more complex interactions in virtually immersive environments. It should be noted that this research focuses on the system's technical implementation and physical-visual consistency validation, and has not yet conducted large-scale user research to quantify its performance in embodied cognition, aesthetic immersion, or interactive intuition. Future work will combine eye-tracking, subjective questionnaires, and behavioral log analysis to evaluate audience perceptual fluency and cognitive engagement in real exhibition environments.

AUTHOR CONTRIBUTIONS

Lu Yang designed, collected and analyzed the data, and drafted the manuscript. Lu Yang conducted the study, critically revised the manuscript for important intellectual content, and gave final approval of the version to be published. Lu Yang participated fully in the work, take public responsibility for appropriate portions of the content, and agreed to be accountable for all aspects of the work in ensuring that questions related to the accuracy or integrity of any part of the work are appropriately investigated and resolved.

CONFLICTS OF INTEREST

The author declares no conflict of interest.

FUNDING

This research received no external funding.

ACKNOWLEDGEMENTS

Not applicable.

REFERENCES

[1] D. Smith-Glaviana, "University students' experience of a digital fashion exhibition: Engagement, embodiment, and object-based learning," Clothing and Textiles Research Journal, vol. 43, no. 1, pp. 32-47, 2025, doi: 10.1177/0887302X231161641.
[2] R. Zhang, F. Peng, and I. Gwilt, "Exploring the role of immersive technology in digitally representing contemporary crafts within hybrid museum exhibitions: a scoping review," Digital Creativity, vol. 35, no. 4, pp. 355-377, 2024, doi: 10.1080/14626268.2024.2398457.
[3] O. Gondoputranto and W. Dibia I, "The use of technology in capturing various traditional motifs and ornaments: A case study of batik fractal, Indonesia and TUDITA-Turkish digital textile archive," Humaniora, vol. 13, no. 1, pp. 39-48, 2022, doi: 10.21512/humaniora.v13i1.7408.
[4] O. Lukovska and T. Kara-Vasylieva, "Mini textile art in Eastern Europe: historical survey," Journal of Visual Art Practice, vol. 21, no. 1, pp. 25-45, 2022, doi: 10.1080/14702029.2021.2020591.
[5] J. Carmen, "Makerspaces: combining information literacy with pattern design for fiber art through digital images," Library trends, vol. 69, no. 3, pp. 585-611, 2021, doi: 10.1353/lib.2021.0005.

[6] S. Pereira and A. Marcos, "Post-digital fashion: the evolution and creation cycle," ZoneModa Journal, vol. 11, no. 1, pp. 71-89, 2021.
[7] O. Zarutska, I. Sydorenko, I. Nebesnyk, et al., "Development of art forms in the contemporary era: New platforms and creative approaches," International Journal on Culture, History, and Religion, vol. 7, no. SI1, pp. 35-51, 2025, doi: 10.63931/ijchr.v7iSI1.101.
[8] E. Macken M, "An overview of recent digital humanities initiatives in US art libraries," Art Libraries Journal, vol. 46, no. 2, pp. 51-56, 2021, doi: 10.1017/alj.2021.5.
[9] L. Du Puis J and C. Yamakawa, "Curating the circus: Collaboration and responsibilities in digital costume exhibitions," Critical Studies in Fashion & Beauty, vol. 13, no. 1, pp. 119-140, 2022, doi: 10.1386/csfb_00040_1.
[10] Y. Ping, "Digital media interactive oil painting art exhibition method based on visual communication," Signal, Image and Video Processing, vol. 18, no. 8, pp. 6239-6250, 2024, doi: 10.1007/s11760-024-03310-1.
[11] G. Stanciel, L. Reddy-Best K, D. Simon J, et al., "Radical structural change in North American dress and textile museums and collections: Critically analyzing social justice, oppression, and empowerment," Clothing and Textiles Research Journal, vol. 42, no. 4, pp. 263-277, 2024, doi: 10.1177/0887302X221132009.
[12] J. Jeong, K. Lee H, and Y. Lee, "Café or art exhibition? Which experience is more effective in luxury fashion flagships? Journal of Fashion Marketing and Management: An International Journal," 2025; 29(2): 252-268, doi: 10.1108/JFMM-12-2022-0269.
[13] L. Impett and F. Offert, "There is a digital art history," Visual Resources, vol. 38, no. 2, pp. 186-209, 2022, doi: 10.1080/01973762.2024.2362466.
[14] O. Koshelieva, O. Tsyselska, O. Kravchuk, et al., "Digital transformation in culture and art: exploring the challenges, opportunities, and implications in Cultural Studies," Research Journal in Advanced Humanities, vol. 4, no. 3, pp. 41-55, 2023, doi: 10.37394/232024.2023.3.4.
[15] M. Kang J Y and H. Lin S, "Building three-dimensional virtual historic fashion museum exhibitions: From the perspective of technology affordances," Clothing and Textiles Research Journal, vol. 43, no. 2, pp. 137-153, 2025, doi: 10.1177/0887302X241257714.
[16] A. Boughlala and A. Smelik, "Tracing the history of digital fashion," Clothing and Textiles Research Journal, vol. 43, no. 3, pp. 171-186, 2025, doi: 10.1177/0887302X241283504.
[17] A. Rochnyak, "Fine art photography as a form of visual art: Aesthetics, styles, and contemporary trends," Art and Design, vol. (2), pp. 93-105, 2025, doi: 10.30857/2617-0272.2025.2.9.
[18] R. Ghoneim and M. Arabasy, "The Role of Artworks of Architectural Design in Emphasizing the Arab Identity," Al-Balqa Journal for Research and Studies, vol. 27, no. 1, pp. 1-14, 2024, doi: 10.35875/1105.027.001.001.
[19] S. Ma, "The politics of curating Japonisme: International art exhibition and soft power in contemporary Japanese cultural diplomacy," Journal of Japonisme, vol. 8, no. 1, pp. 31-66, 2023, doi: 10.1163/24054992-08010001.
[20] U. Suhud, R. Sulistyowati, D. SugiantoSitohang, et al., "Assessing the attention-interest-search-action-share (AISAS) model on the traditional textile exhibition visitors," Environment and Social Psychology, vol. 9, no. 7, pp. 2082-2082, 2024, doi: 10.59429/esp.v9i7.2082.
[21] P. Chamarty, "Kalamkari and Chintz: A post-colonial reassessment of entangled textile histories," DISCERN: International Journal of Design for Social Change, Sustainable Innovation and Entrepreneurship, vol. 5, no. 1, pp. 40-53, 2024.
[22] F. Bertacchini, S. Pantano P, and E. Bilotta, "From science to art forms: exploring design, creativity and innovation through chaos physicalization," International Journal of Design Creativity and Innovation, vol. 12, no. 1, pp. 23-60, 2024, doi: 10.1080/21650349.2023.2285485.
[23] Q. Dou, "Virtual Fashion: Production and Display," The Frontiers of Society, Science and Technology, vol. 6, no. 7, pp. 141-152, 2024, doi: 10.25236/FSST.2024.060720.
[24] Y. Ong C and L. Wai Ching Deanna, "Emerging stronger from COVID-19 through arts," Global Health Promotion, vol. 30, no. 2, pp. 28-34, 2023, doi: 10.1177/17579759221118256.
[25] M. Xepoleas L and E. Hayflick, "Curating costumes from many lands: Addressing the colonial gaze in two university dress collections through digital curation," Critical Studies in Fashion & Beauty, vol. 13, no. 1, pp. 21-43, 2022, doi: 10.1386/csfb_00036_1.
[26] J. Parsons and K. Morris, "Apparel and textile design scholarship: shared knowledge, dissemination, and evaluation," Clothing and Textiles Research Journal, vol. 39, no. 1, pp. 7-23, 2021, doi: 10.1177/0887302X20903809.
[27] O. Yezhova, J. Zhao, and K. Pashkevych, "Exploring Design Aspects of Online Museums: From Cultural Heritage to Art, Science and Fashion," Preservation, Digital Technology & Culture, vol. 54, no. 1, pp. 35-50, 2025, doi: 10.1515/pdtc-2024-0044.
[28] C. Guo, X. Zhang, and Z. Gao, "Application of Virtual Reality Technology Based on Convolutional Neural Network in Digital Media Art Creation," International Journal of Cognitive Informatics and natural intelligence (ijcini), vol. 18, no. 1, pp. 1-17, 2024, doi: 10.4018/IJCINI.353915.
[29] B. Marcketti S and F. Gordon J, "The fashion and textiles collection matrix: A proposed self-assessment tool," Critical Studies in Fashion & Beauty, vol. 13, no. 1, pp. 167-183, 2022, doi: 10.1386/csfb_00042_1.
[30] L. Lan and P. Liu, "Exhibiting fashion on the heritage site: the interrelation between body, heritage space, and fashionable clothing," Humanities and Social Sciences Communications, vol. 10, no. 1, pp. 1-12, 2023, doi: 10.1057/s41599-023-02373-8.
[31] K. Howard E, K. Asinyo B, K. Seidu R, et al., "Digital imitation of batik, tie-dye and weave effects for manual screen printing," Journal of Design Research, vol. 20, no. 2, pp. 142-158, 2022, doi: 10.1504/JDR.2022.127567.
[32] D. Brown, "Correspondence, not just Transaction: Exhibiting Asian Art Collections at the Art Gallery of NSW," Southeast of Now: Directions in Contemporary and Modern Art in Asia, vol. 7, no. 2, pp. 165-178, 2023, doi: 10.56159/sen.2023.a916552.
[33] M. Paatela-Nieminen, "Remixing real and imaginary in art education with fully immersive virtual reality," International Journal of education through art, vol. 17, no. 3, pp. 415-431, 2021, doi: 10.1386/eta_00077_1.
[34] N. Haqqi M H and R. Harjanto, "Exploring generation z's fascination with Jakarta art museum through social media contents," Jurnal Studi Komunikasi, vol. 9, no. 1, pp. 123-138, 2025, doi: 10.25139/jsk.v9i1.9200.
[35] M. Lin, "A brief introduction to body-oriented parametric design for 3D-printed fashion and textiles," Textile, vol. 20, no. 1, pp. 55-73, 2022, doi: 10.1080/14759756.2021.1955582.
[36] A. Dragojlovic and L. Quinan C, "Queering and decolonising the museum: 'In the Presence of Absence' exhibition at the Stedelijk Museum," Memory Studies, vol. 16, no. 1, pp. 161-165, 2023, doi: 10.1177/17506980221143708.